Small amplitude modelling of acoustic damping cavities

Geoffrey Searby

Small amplitude modelling of acoustic damping cavities

Geoff Searby
CNRS-IRPHE and ONERA Consultant
49 rue F. Joliot-Curie
Technopole de Chateau-Gombert
13384 MARSEILLE France

Abstract
We will first recall the classical results for the laminar dissipation of acoustic energy in the boundary layer of a forced resonator. We then show how this result can be used in conjunction with a Helmholtz solver to calculate the laminar damping of a cavity of arbitrary geometry. The approach is validated by application to a trivial geometry for which the result is known analytically (HF1 step 1). We then present the results for the remaining test cases (HF1 steps 2, 3 and 4). The computational effort is lightweight, ranging from a few seconds of cpu time for step one to a few minutes for the 3-D case, step 4. These test cases are non-reacting, but the approach can be extended to accommodate strong temperature variations, provided the temperature and density fields are known. Finally we discuss the limitations of this approach and possible reasons for differences between these calculations, full DNS calculations, and experimental measurements on real chambers.

1 Introduction

High frequency instability in liquid-fuelled rocket engines is still an open problem [1, 2]. Various methods have been used to increase the dissipation rate of acoustic disturbances in rocket engine combustion chambers with the objective of increasing the stability margin of the motors. Among the well known damping devices are baffles, acoustic liners and quarter-wave resonators. These devices are conceptually simple. Quarter-wave cavities are known to be efficient to increase the stability margin when placed close to the injection plate. However these devices have a relatively narrow dissipation bandwidth and each cavity needs to be tuned to a specific chamber resonance. The optimum tuning of damping cavities cavities and the associated acoustic damping can be calculated analytically only for trivial geometries. For realistic geometries it is necessary to resort to numerical simulation. In this paper we present a simple time-domain method to estimate the damping rate of an arbitrary geometry.

Two distinct damping mechanisms are associated with acoustic dampers. The first mechanism arises from viscous drag and heat transfer at the cavity walls. This is a linear mechanism, and the associated acoustic resistance is independent of the acoustic amplitude. This mechanism dominates at low acoustic amplitudes and it is important for the linear stability of propulsion devices. The second mechanism arises from the formation of vortex eddies at the exit from the damping cavity. This is a nonlinear mechanism and the associated acoustic resistance increases with the velocity of the flow at the entrance to the cavity[3, 4, 5]. The latter mechanism dominates at high acoustic amplitudes and determines the dynamic stability characteristics. The relative contribution of these two mechanisms described by the acoustic Strouhal number $\mathrm{St}_{ac} = \omega R/\hat{u}$, where R is the radius of the cavity exit and $\hat{u}$ is the amplitude of the acoustic velocity at the cavity exit[6]. For $\mathrm{St}_{ac} \gg 1$ the viscous mechanisms dominate. Since the two mechanisms are physically independent, the associated acoustic resistances are additive, at least up to moderately non-linear acoustic levels.

This paper is concerned only with the linear viscous and thermal damping. We first recall the classical results for laminar energy dissipation in the boundary layer of a forced resonator. We then show how this result can be used to calculate the laminar damping of a cavity of

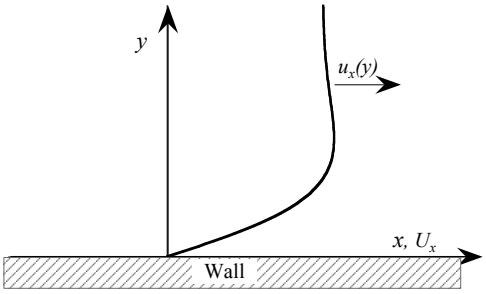

Figure 1: Typical velocity profile in an acoustic boundary layer.

arbitrary geometry, with the help of a lightweight Helmholtz solver. This approach is validated on a closed cylindrical cavity, for which the analytical solution is known (HF1 step 1). We then apply the method to the 2–D test case (HF1 steps 2 and 3), where we will give more detailed results than requested. Finally the method is applied to the fully 3–D case, HF1 step 4. In the conclusion we will discuss some possible limitations of the method. The approach described here is presented in more detail in a paper published recently in the Journal of Propulsion and Power [7].

2 Laminar boundary layer theory

Viscous and thermal losses at the walls are diffusive and obey qualitatively identical laws. The viscous dissipation is proportional to the product of the velocity gradient at the wall and the shear viscosity. The thermal dissipation is proportional to the product of the temperature gradient at the wall and the thermal conductivity.

2.1 Viscous losses

The viscous loss in an acoustic cavity was first calculated by Stokes [8]. Here we will use the boundary layer formulation given by G.K. Batchelor [9]. We consider only the (quasi-)steady state situation, where any time dependence is on a scale long compared to the acoustic period.

We consider a plane infinite wall immersed in a semi-infinite fluid. The y coordinate is normal to the wall, see figure 1. Let the bulk of the fluid, oscillate with velocity $u = \hat{u}_x \cos(\omega t)$ along the x axis, in a plane parallel to the wall. If transient effects are neglected, and if the velocity gradients parallel to the wall are negligible (i.e. if the acoustic wavelength is very large compared to the thickness of the acoustic boundary layer) then it can be shown that the unsteady velocity profile in the liquid is given by

$$u'(y,t) = \hat{u}_x \left[\exp\left(-\frac{y}{\delta_\nu}\right) \cos\left(\omega t - \frac{y}{\delta_\nu}\right) - \cos\left(\omega t\right) \right], \tag{1}$$

where δ_ν is a measure of the thickness of the unsteady viscous boundary layer

$$\delta_\nu = \sqrt{\frac{2\nu}{\omega}}, \tag{2}$$

ν is the kinematic viscosity and ω is the angular frequency. The velocity in the fluid oscillates with a "wavelength" $2\pi\sqrt{2\nu/\omega}$. A typical order of magnitude for the thickness of an acoustic boundary layer is 100μm

The force per unit area exerted by the wall on the liquid is given by $F = \rho\nu(\partial u'/\partial y)\,|_{y=0}$ and so

$$F = \rho\nu\frac{\hat{u}_x}{\delta_\nu}\left(\sin(\omega t) - \cos(\omega t)\right) \tag{3}$$

It is interesting to note that the force is *not* in phase with the velocity in the bulk of the fluid ($u = \hat{u}_x\cos(\omega t)$): there is a resistive (in phase) component and a reactive (90° phase lag) component. Averaged over an acoustic period, only the resistive component contributes to energy dissipation ($\mathrm{d}E_s/\mathrm{d}t = F\hat{u}_x$).

$$\left\langle\frac{\mathrm{d}E_s}{\mathrm{d}t}\right\rangle_\nu = \frac{1}{2}\rho\nu\frac{u_x^2}{\delta_\nu} \tag{4}$$

$$= \frac{1}{2}\rho u_x^2\sqrt{\frac{\omega\nu}{2}}, \tag{5}$$

where E_s is the energy per unit area.

The total rate of energy dissipation by viscous forces in an acoustic cavity can then calculated by integrating equ.(5) over all the solid walls

$$\left\langle\frac{\mathrm{d}E}{\mathrm{d}t}\right\rangle_\nu = \int_S\left\langle\frac{\mathrm{d}E_s}{\mathrm{d}t}\right\rangle_\nu \mathrm{d}S. \tag{6}$$

2.2 Thermal losses

Acoustic oscillations are adiabatic if the wavelength, λ, satisfies $\lambda > 2\pi D_{th}/c \approx 0.5\,\mu\mathrm{m}$, where D_{th} is the thermal diffusivity and c is the speed of sound. In combustion chambers this inequality is always true, so the acoustic pressure oscillations give rise to temperature oscillations:

$$\delta T = \frac{\gamma - 1}{\gamma}\frac{T_0}{P_0}p \tag{7}$$

where T_0 and P_0 are the average temperature and pressure respectively, p is the oscillating acoustic pressure, $P = P_0 + p\sin(\omega t)$, and γ is the ratio of specific heats. In the presence of an isothermal wall there will be an oscillating heat flux to the wall. This heat flux is irreversible and also contributes to energy dissipation. The calculation for the unsteady heat flux proceeds in a similar way to the calculation of the unsteady viscous stress and was calculated by Nielsen [10]. The final result for the rate of energy loss per unit area is:

$$\left\langle\frac{\mathrm{d}E_s}{\mathrm{d}t}\right\rangle_{th} = \frac{1}{2}\frac{\gamma - 1}{\gamma}\frac{p^2}{P_0}\sqrt{\frac{\omega D_{th}}{2}} \tag{8}$$

where D_{th} is the thermal diffusivity. For a perfect gas, the sound velocity is related to the mean pressure $P_0 \equiv (\rho c^2)/\gamma$ and in this case equ.(8) is easily written in a form that is symmetrical to equ.(5):

$$\left\langle\frac{\mathrm{d}E_s}{\mathrm{d}t}\right\rangle_{th} = \frac{1}{2}(\gamma - 1)\frac{p^2}{\rho c^2}\sqrt{\frac{\omega D_{th}}{2}} \tag{9}$$

2.3 Damping rate

The total rate of acoustic energy dissipation in the system can be calculated by integrating expressions (5) and (9) over the walls acoustic system.

$$\left\langle\frac{\mathrm{d}E}{\mathrm{d}t}\right\rangle_{\mathrm{Total}} = \int_S\left\langle\frac{\mathrm{d}E_s}{\mathrm{d}t}\right\rangle_\nu \mathrm{d}S + \int_S\left\langle\frac{\mathrm{d}E_s}{\mathrm{d}t}\right\rangle_{th}\mathrm{d}S \tag{10}$$

To be rigorous, it is necessary integrate not only over both the walls of the damping cavity, but also over the walls of the combustion chamber. To evaluate these integrals, is is sufficient to know local amplitude of the acoustic velocity and pressure oscillations in front of the wall, but outside the acoustic boundary layer. In the following, we will use that the acoustic amplitudes calculated for non-stick (slip) adiabatic walls. This approximation will be good if the acoustic damping is not too large.

The total acoustic energy in the system can be calculated integrating the kinetic energy, $(1/2)\rho u^2$ and the potential energy, $(1/2)p^2/(\rho c^2)$ over the volume of the acoustic system:

$$E = \frac{1}{T}\int_T \int_V \left(\frac{1}{2}\rho u^2(x,t) + \frac{1}{2}\frac{p^2(x,t)}{\rho c^2} \right) \mathrm{d}V\, \mathrm{d}t. \tag{11}$$

The integration is over one period of oscillation, $T = 2\pi/\omega$, and over the volume of the cylinder, $\mathrm{d}V \equiv S\mathrm{d}x$.

The damping rate of *energy* in the system is then given by the ratio of the energy dissipation rate to the total energy:

$$\sigma_E = \frac{1}{E}\frac{\mathrm{d}E}{\mathrm{d}t} \tag{12}$$

Note that the damping rate of the *pressure*, σ_p, is one-half this quantity

$$\sigma_p = \frac{1}{2E}\frac{\mathrm{d}E}{\mathrm{d}t}. \tag{13}$$

The damping rate calculated this way is independent of the amplitude of the acoustic wave used to perform the calculations.

3 Test case step 1: Application to a cylindrical resonator

We apply the above results to a cylindrical resonator closed at both ends. The cavity is directed along the x axis, and is closed at $x = 0, L$. If the attenuation is weak then the pressure and velocity in a standing wave can be written

$$\begin{aligned} p(x,t) &= \Re\left[\hat{p}\cos(kx)\exp(-\mathrm{i}\omega t)\right] \\ u(x,t) &= -\Im\left[\mathrm{i}\hat{u}\sin(kx)\exp(-\mathrm{i}\omega t)\right] \\ \hat{p} &= \rho c\hat{u} \end{aligned} \tag{14}$$

where $\hat{u}$ and $\hat{p}$ are the peak amplitudes of the oscillations at the anti-nodes of velocity and pressure respectively. If the attenuation is weak, they may be considered constant during a period of oscillation. The integral equ.(11) is then easily evaluated to give:

$$E = \pi R^2 L\,\frac{1}{4}\rho\hat{u}^2 \equiv \pi R^2 L\,\frac{1}{4}\frac{\hat{p}^2}{\rho c^2}. \tag{15}$$

Viscous contribution

The viscous contribution to damping is given by the integral of equ.(5) over the side walls of the cylinder. There is no contribution from the end walls, since the velocity there is zero.

$$\left\langle \frac{\mathrm{d}E}{\mathrm{d}t} \right\rangle_\nu = \pi R L \frac{1}{2}\rho\hat{u}^2\sqrt{\frac{\omega\nu}{2}}. \tag{16}$$

The viscous contribution to the damping rate, $\sigma_\nu \equiv (1/E)(\mathrm{d}E/\mathrm{d}t)_\nu$ is then

$$\sigma_\nu = \frac{2}{R}\sqrt{\frac{\omega\nu}{2}}. \tag{17}$$

Thermal contribution

The thermal contribution to damping is given by the integral of equ.(9) over the side walls of the cylinder. The integral must also be evaluated at the end wall(s), if the cylinder is closed, since these locations are anti-nodes for the oscillations of pressure and temperature.

$$\left\langle \frac{\mathrm{d}E}{\mathrm{d}t} \right\rangle_{th} = \pi RL\ (\gamma - 1)\,\frac{1}{2}\frac{\hat{p}^2}{\rho c^2}\sqrt{\frac{\omega D_{th}}{2}}\left(1 + \frac{2R}{L}\right). \tag{18}$$

The thermal contribution to the damping rate is then:

$$\sigma_{th} = \frac{2(\gamma - 1)}{R}\sqrt{\frac{\omega D_{th}}{2}}\left(1 + \frac{nR}{L}\right) \tag{19}$$

If the aspect ratio of the cylinder is high $L \gg R$, then the contribution from the end wall(s) can be neglected.

Total damping of a cylindrical resonator

The total damping rate of energy is just the sum of the viscous and thermal contributions, $\sigma_e = \sigma_\nu + \sigma_{th}$

$$\sigma_e = \frac{2}{R}\left[\sqrt{\frac{\omega\nu}{2}} + (\gamma - 1)\sqrt{\frac{\omega D_{th}}{2}}\left(1 + \frac{nR}{L}\right)\right] \tag{20}$$

Equation (20) gives the damping rate of *energy* in the cavity. The damping rate of *pressure* is one half the damping rate of energy :

$$\sigma_p = \frac{1}{R}\sqrt{\frac{\omega\nu}{2}}\left[1 + \left(\frac{\gamma - 1}{\sqrt{\mathrm{Pr}}}\right)\left(1 + \frac{nR}{L}\right)\right], \tag{21}$$

where we have expressed the thermal diffusivity in terms of the viscosity and the Prandtl number. This expression is valid for weak damping. Equivalent expressions have been obtained by other authors, such as Tijdeman[11], using a more rigorous formulation. A. Nicole [12] has obtained an implicit equation for the resonant frequency and damping rate of a cylindrical cavity with arbitrary strong viscous damping, however the thermal contribution was not taken into account. Nicole's expression reduces to (17) for weak damping and a thin boundary layer, $\sigma_\nu/\omega \ll 1$ et $\delta/R \ll 1$.

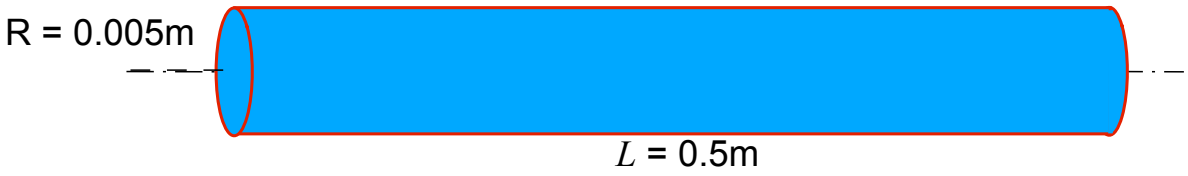

Figure 2: Geometry of the closed cylindrical cavity

T (K)	2100.	c (m/s)	1884.5
ρ (kg/m^3)	0.358	γ	1.27
μ (kg/m/s)	$4.833\,10^{-5} \times 50$	ν (m^2/s)	$1.35\,10^{-4} \times 50$
C_p (J/kg/K)	6257.6	Pr	∞ (adiabatic walls)

Table 1: Gas properties used to calculate the damping of a closed cylinder

The geometry of the cylinder used in step 1 is shown in figure 2. Note that the aspect ratio of the cylinder has been greatly deformed: the real aspect ratio is 50:1. Table 1 shows the gas properties used in the calculations. The undamped eigenfrequency of the cylinder is just

$$\text{Undamped eigenfrequency} \quad f_0 = \frac{c}{2L} = 1884.5\,\text{Hz}.$$

Using the values in table 1, the analytical value (equation (21)) of the pressure damping rate of the cylindrical cavity (figure 2) is found to be:

$$\text{Analytical damping rate} \quad \sigma_p = 1264.3\,\text{s}^{-1}.$$

To first-order, the frequency of the damped cavity, f can be obtained from the undamped eigenfrequency f_0 using the relation $f = f_0 - \sigma_p/(2\pi)$:

$$f = \left(f_0 - \frac{\sigma_p}{2\pi}\right) = 1683.3\,\text{Hz}.$$

In the next section we will show how a numerical Helmoltz solver can be used to obtain the damping in an arbitrary geometry. This numerical solver has been validated on the present geometry. The results are: undamped eigenfrequency = 1884.50 Hz, pressure damping rate = 1264.31 s^{-1}, in perfect agreement with the underlying analytical model. The damping rate given in equation (equation (21) was derived under the double approximation that

- The cavity diameter is very much larger than the thickness of the acoustic boundary layer
- The damping rate is negligible compared to the eigenfrequency of the chamber

These limitations are generally well verified in real-life systems, however in this particular test case, neither approximation is well verified. In particular the damping rate is far from negligible compared to the eigenfrequency. A. Nicole [12] has performed a more rigorous analytical calculation for a cylindrical cavity with arbitrarily strong viscous damping (but excluding the thermal contribution). Application of this implicit result to the present case gives: damped frequency = 1686.0 Hz, pressure damping rate = 1413.3 s^{-1}. these "exact" results are a little different to the results obtained using the above analysis for weak daming. However the two analyses converge rapidly for more realistic (smaller) values of viscosity.

The three sets of results: analytical, numerical (both based on the same approach) and the "exact" result of A. Nicole are summarised in table 2.

	Analytical	Numerical	"Exact"
Undamped frequency, f_0	1884.5 Hz	1884.5 Hz	1884.5 Hz
Damped frequency, $f_0 - \sigma_p/(2\pi)$	1683.3 Hz	1683.3 Hz	1686.0 Hz
Damping rate, σ_p	1264.3 s^{-1}	1264.3 s^{-1}	1413.3 s^{-1}

Table 2: Results for step 1

4 Test case step 2: Application to axisymmetric coupled resonators

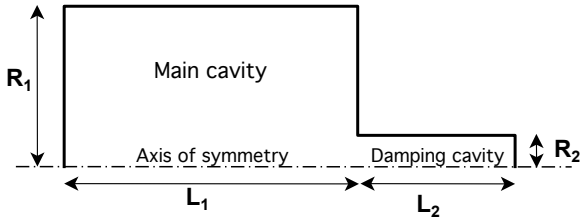

Figure 3: Geometry of the two coupled cylindrical cavities

Analytical expressions, such as (14), for the acoustic field can be found only for trivial geometries and are not available for more realistic geometries. To the best of my knowledge even the simple geometry shown in figure 3 does not have a known analytical solution. However it is possible to obtain a numerical solution using a standard software tool to solve the Helmholtz equation.

4.1 The Helmholtz equation

The standard wave equation (d'Alembert's equation) for small amplitude acoustic propagation in a lossless medium is

$$\frac{\partial^2 p}{\partial t^2} - c^2 \boldsymbol{\nabla}^2 p = 0, \tag{22}$$

where p is the unsteady acoustic pressure and c is the speed of sound in the medium. If the acoustic oscillation is harmonic and quasi-stationary, such as at resonance, the spatial and time dependencies of the acoustic field can be separated:

$$p(\mathbf{x}, t) = \hat{p}(\mathbf{x}) \exp(-\mathrm{i}\omega t).$$

The space-dependent part, $\hat{p}(\mathbf{x})$, of the acoustic pressure field must then satisfy Helmholtz's equation:

$$\boldsymbol{\nabla}^2 \hat{p}(\mathbf{x}) + \frac{\omega^2}{c^2} \hat{p}(\mathbf{x}) = 0 \tag{23}$$

This differential equation is easily solved using standard software tools. The necessary inputs are

- The speed of sound (which can be a function of position)
- The boundary conditions

The outputs are

- The eigenfrequencies, ω_n of the geometry defined by the boundary conditions
- The pressure field $\hat{p}(\mathbf{x})$ and the velocity field $\hat{u}(\mathbf{x})$

where

$$\hat{u}(\mathbf{x}) \equiv \frac{i}{\omega_n \rho} \boldsymbol{\nabla} \hat{p}(\mathbf{x}).$$

The numerical solutions for the pressure and velocity fields can then be used as before to calculate the total energy in the system:

$$E = \frac{1}{2}\int_V \left(\frac{1}{2}\rho\hat{u}^2(\mathbf{x}) + \frac{1}{2}\frac{\hat{p}^2(\mathbf{x})}{\rho c^2}\right) r\,\mathrm{d}r\,\mathrm{d}\theta \tag{24}$$

and the total energy dissipation at the walls:

$$\frac{\mathrm{d}E}{\mathrm{d}t} = \frac{1}{2}\sqrt{\frac{\omega_n\nu}{2}}\int_S \left(\rho\hat{u}_s^2(\mathbf{x}) + \frac{(\gamma-1)}{\sqrt{\mathrm{P}r}}\frac{\hat{p}_s^2(\mathbf{x})}{\rho c^2}\right)\mathrm{d}s \tag{25}$$

where $\hat{u}_s$ and $\hat{p}_s$ are the values of the velocity and pressure at the walls. The pressure damping rate is then given by equation (13). The solutions to the Helmholtz equation can be obtained in a few seconds for a simple 2–D geometry, or in a few minutes for a 3–D geometry.

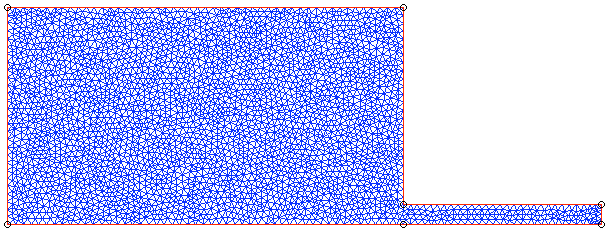

Figure 4: Typical mesh for the geometry of figure 3.

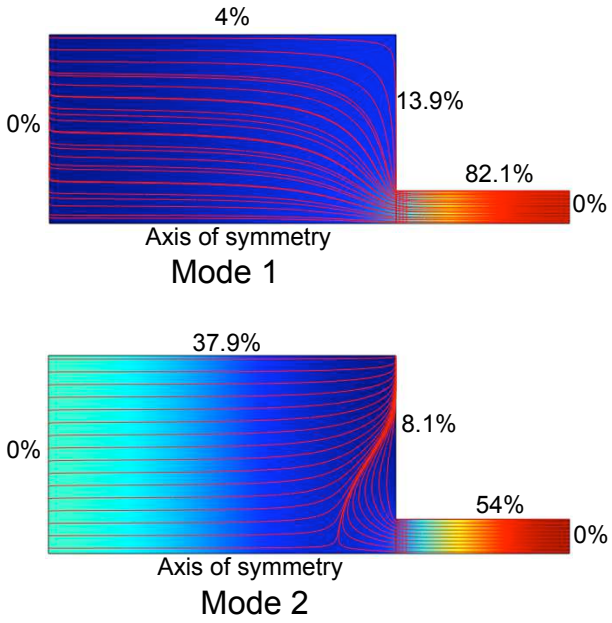

Figure 5: Typical acoustic pressure fields for the geometry of figure 3. $L_1 = 0.2\,\mathrm{m}$ $L_2 = 0.2\,\mathrm{m}$ $L_1 = 0.1\,\mathrm{m}$ $R_1 = 0.11\,\mathrm{m}$ $R_2 = 0.019\,\mathrm{m}$

In the following sections of this paper, the Helmholtz equation has been solved using a commercial PDE solver called COMSOL. The domain has an unstructured triangular mesh. For 2–D axisymmetric geometry of step 2, typically 6 000 to 7 000 cells were used, depending

on the size of the damping cavity. A typical mesh is shown in figure 4. Figure 5 shows typical solutions for the pressure fields of the first and second acoustic modes of the geometry of figure 3. The flow streamlines are shown in red and the relative contributions for the damping from each wall are also indicated. Since the walls are designated as adiabatic in this test, there is no thermal dissipation and the two extremities do not contribute to the damping. It is interesting to note that, for the second acoustic mode, the damping on the main cavity walls represents 46% of the total damping.

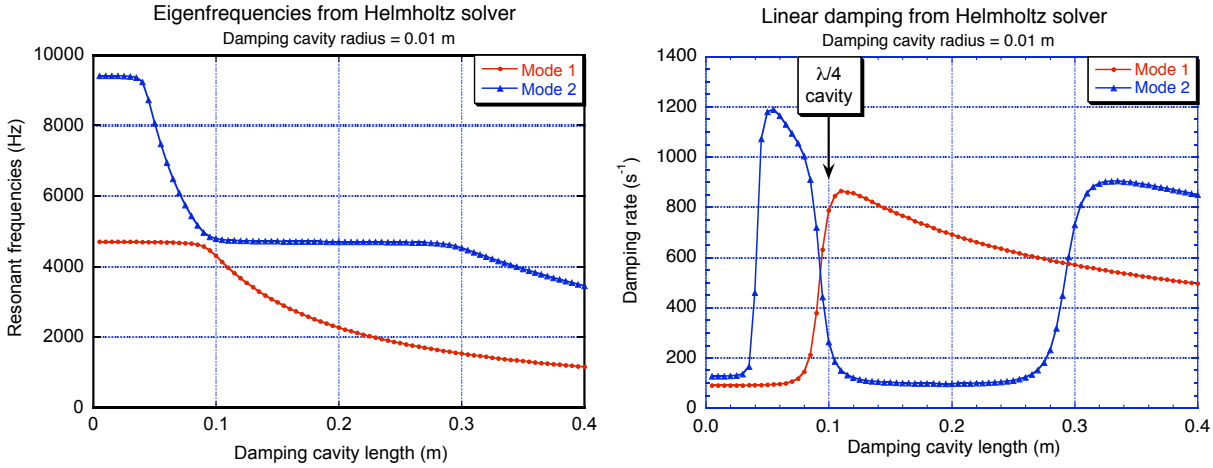

Figure 6: Evolution of the resonant frequencies and damping rates as functions of damping cavity length. $L_1 = 0.2\,\mathrm{m}$ L_2 variable $R_1 = 0.11\,\mathrm{m}$ $R_2 = 0.01\,\mathrm{m}$.

Although not requested as part of this test case, figure 6 shows the undamped eigenfrequencies and the damping rates of the first two modes as a function of the length of the damping cavity, for a damping cavity radius $R_2 = 0.01\,\mathrm{m}$. The properties of the gas in the system are given in table 1. The resonant frequencies of the coupled system are, in general, different to those of the isolated components. The resonant frequencies evolve in a very non-linear manner with a change in the length of the damping cavity. This behaviour is generic, and is consistent with a simple quasi 1–D analytical model of two coupled cavities [13]. It will be seen that the resonant frequencies of the CRC evolve in a similar manner with the length of the damping cavity. The evolution of the damping rates of the first two modes is shown in the right graph of figure 6. The $\lambda/4$ tuning is not optimal for the damping of mode 1. In fact it is a dangerous tuning since the damping rate varies very quickly with cavity length (or with a change in sound speed in the main cavity). A better tuning for damping mode 1 would be $\lambda/3.5$ ($L_2 = 0.115\,\mathrm{m}$) instead of $\lambda/4$. Another interesting tuning is $\lambda/1.3$ ($L_2 = 0.320\,\mathrm{m}$). For this cavity length, mode 1 is almost as strongly damped as with the $\lambda/4$ tuning, but mode 2 is also strongly damped and moreover the damping rates of both modes are relatively insensitive to cavity length.

Figure 7 shows the evolution of the frequencies and damping of the first two modes as a function of the damping cavity radius. The length of the damping cavity is 0.1 m, corresponding to the "standard" $\lambda/4$ tuning with respect to he first mode of the main cavity.

Mode 1 is more strongly damped than mode 2. A closer investigation shows that the reason for this difference is that the relative acoustic amplitude in the damping cavity is systematically higher or mode one than for mode 2, leading to a higher dissipation in the damping cavity.

The results predict that the total damping rate increases as the radius of the damping cavity is decreased. The physical reason for this is that the resulting increase in relative acoustic

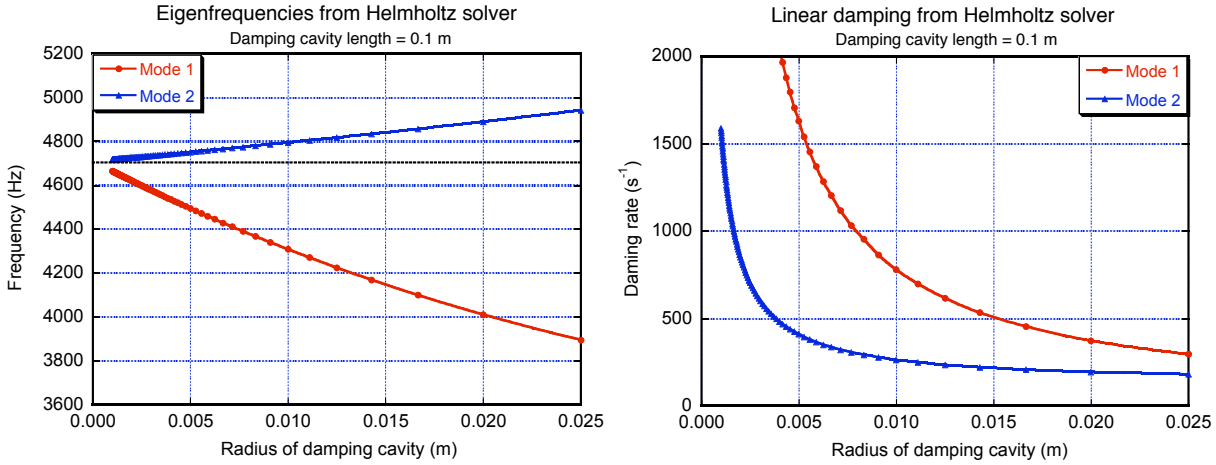

Figure 7: Evolution of mode frequencies and damping rate as functions of damping cavity radius. $L_1 = 0.2\,\mathrm{m}$ $L_2 = 0.1\,\mathrm{m}$ $R_1 = 0.11\,\mathrm{m}$ R_2 variable.

intensity inside damping cavity more than overweighs the decrease in surface area. Obviously, this trend cannot continue indefinitely and the semi-analytical result will fail at small cavity radii when boundary layer thickness becomes comparable to cavity radius.

The results requested for this test case are summarised in table 3, where the undamped eigenfrequencies of figure 7 have been corrected for damping using the relation $f = f_0 - \sigma_p/(2\pi)$.

	$R = 5\,\mathrm{mm}$			$R = 10\,\mathrm{mm}$		
	Frequency Hz		σ_p	Frequency Hz		σ_p
	eigenvalue	corrected	s^{-1}	eigenvalue	corrected	s^{-1}
Mode 1	(4495)	4235	1631	(4309)	4185	779
Mode 2	(4752)	4687	411	(4796)	4754	263

Table 3: Results for step 2

5 Test case step 3: Application to a 2–D model of the CRC

The CRC, or Common Research Chamber, is a small aspect ratio cylindrical chamber equipped with a lateral damping cavity. The chamber radius is $R_c = 100\,\mathrm{mm}$ and the chamber depth is $H_c = 42\,\mathrm{mm}$. It is modelled here in 2–D as a circle of radius 100 mm equipped with a rectangular damping cavity of width $W_R = 10\,\mathrm{mm}$ and variable length between $L_R = 0\,\mathrm{mm}$ and $L_R = 160\,\mathrm{mm}$. The geometry is shown in figure 8. The gas properties used in the simulations are the same as the properties given in table 1, expect for the viscosity which was set to $\mu = 10\mu_0$ instead of $\mu = 50\mu_0$. The chamber and cavity walls were adiabatic, except for the last calculation.

Figure 9 shows the evolution of the undamped eigenfrequencies of the first 8 modes of the chamber as a function of the length of the damping cavity. The modes are labelled according to their "parent" mode, meaning the structure of the mode when the cavity length tends to zero. The presence of the damping cavity breaks the cylindrical symmetry of the chamber. For each of

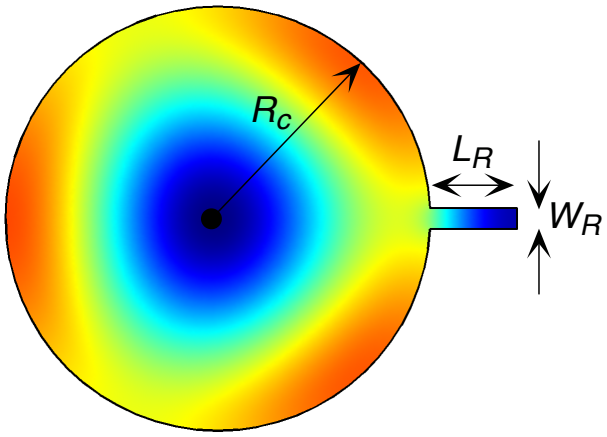

Figure 8: Geometry of the 2–D mode of the CRC. $R_c = 0.1\,\mathrm{m}$, $W_R = 0.01\,\mathrm{m}$, L_R variable.

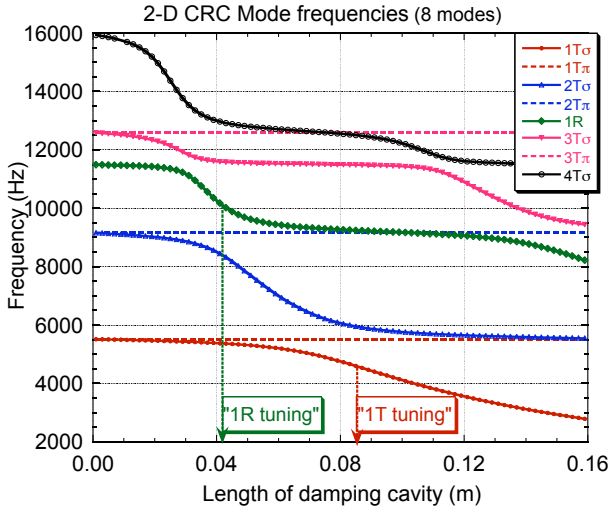

Figure 9: Frequencies of the first 8 modes of the 2–D CRC as a function of cavity length

the transverse modes of the chamber, the orientationally degenerate mode for $L_R = 0$ is broken into two distinct modes, labelled nT_σ, and nT_π. the "π" modes have a pressure node aligned with the axis of the damping cavity. There is no flow into or out of the cavity, and the frequency of the mode is not affected by the presence of the cavity. The "σ" modes are orthogonal to the "π" modes. They have a pressure anti-node aligned with the axis of the damping cavity, and they are strongly affected by its length. The modes with a radial parent do not have a "π" form and also change in frequency with the length of the cavity.

Changing the length of the damping cavity changes not only the frequency of the "σ" modes, but also their geometrical shape. For example, the mode shown in figure 8 has a "1R" parent mode (the green curve in figure 9) Here the cavity length has appproximately the "1R" tuning, however when the cavity length is increased to 100 mm, the frequency of the mode has drops to that of the 2T mode of an unperturbed disk, and the mode shape is also that of the 2T mode of an unperturbed disk. However, for an arbitrary cavity length, the "σ" modes have intermediate shapes that are totally different from any unperturbed transverse mode. For mode detailed explanations, see reference [13]. The general evolution of mode frequencies with cavity length is similar to that of figure 6. The change in frequency is nonlinear with rapid changes for certain lengths of the cavity.

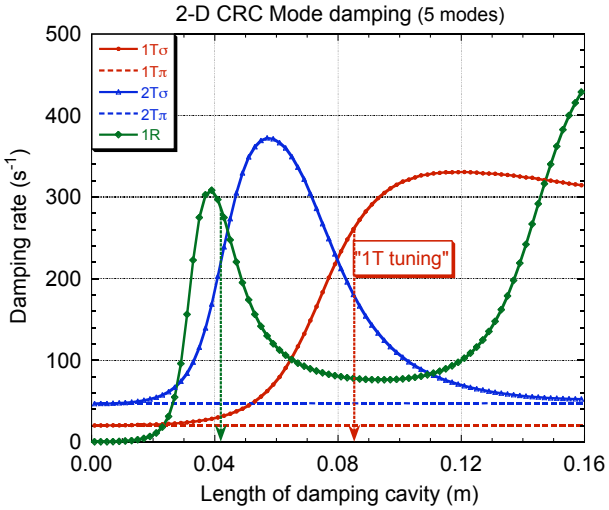

Figure 10: Damping of the first 5 modes of the 2–D CRC as a function of cavity length

Figure 10 shows the damping rate of the first five modes of 2–D CRC as a function of the cavity length. All the walls are adiabatic. The two arrows show the length of the damping cavities requested for this test case. The results are qualitatively similar to those found for the axisymmetric coupled cavities. Again, the so-called $\lambda/4$ tuning, with $L_R = 85$ mm, is not optimal to damp the 1Tσ mode. A cavity length of $L_R = 120$ mm will give a higher damping and also a better tolerance to a tuning error.

The results request for this step are summarised in table 4. The frequencies given in the table are the eigenfrequencies corrected for damping. The first-order correction, $f = f_0 - \sigma_p/(2\pi)$, has been used .

	Adiabatic walls				Isothermal walls	
	$L = 41$ mm		$L = 85$ mm		$L = 41$ mm	
Mode	Freq. Hz	σ_p s^{-1}	Freq. Hz	σ_p s^{-1}	Freq. Hz	σ_p s^{-1}
$1T_\sigma$	5373	30	4559	261		
$2T_\sigma$	8417	203	5927	181	8400	305
$3T_\pi$	12595	77	12595	77		

Table 4: Results for step 3

6 Test case step 4: Application to a 3–D model of the CRC

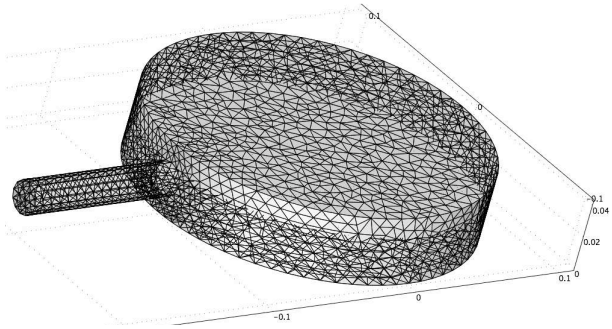

Figure 11: Unstructed mesh used in the 3–D model of the CRC

The CRC has been modelled in full 3–D. The chamber radius is $R_c = 100$ mm, and the chamber height is $H_c = 42$ mm. The damping cavity has a fixed radius of 5 mm and a length that has been varied from 0 mm to 160 mm. Since the objective here is to simulate the damping of a real combustion chamber, all the walls are isothermal. The mesh is unstructured with typically 70 000 to 80 00 cells, depending in the length of the damping cavity. The execution time of the Helmholtz solver on a laptop computer was approximately 5 minutes per geometry, including post-processing to obtain the damping rates. Figure 11 shows the mesh geometry.

T (K)	293.	c (m/s)	345
ρ (kg/m^3)	1.20	Pr	0.773
μ (kg/m/s)	$2.04\,10^{-5}$	ν (m^2/s)	$1.70\,10^{-5}$

Table 5: Gas properties (ambient air) used to calculate the damping of the 3–D CRC

The properties of the gas used in these calculations are shown in table 5. They correspond to the properties of ambient air at 20°C. Figure 12 shows the first six eigenfrequencies of the 3–D CRC as a function of the cavity length. These frequencies are undamped eigenfrequencies, they have not been corrected for damping. The behaviour is qualitatively identical to those of the axisymmetric coupled chambers (figure 6), and of the 2–D CRC (figure 9). The presence of the damping cavity breaks the orientationally degenerate transverse modes into "π" modes that are insensitive to the cavity length, and "σ" modes whose frequencies vary strongly with the cavity length. The mode frequencies do not change linearly with cavity length, but tend to change rapidly for certain critical lengths of of the cavity. The modes have been labelled according to

the shape of the "parent" mode, i.e. the shape of the mode as the length of the cavity tends to zero.

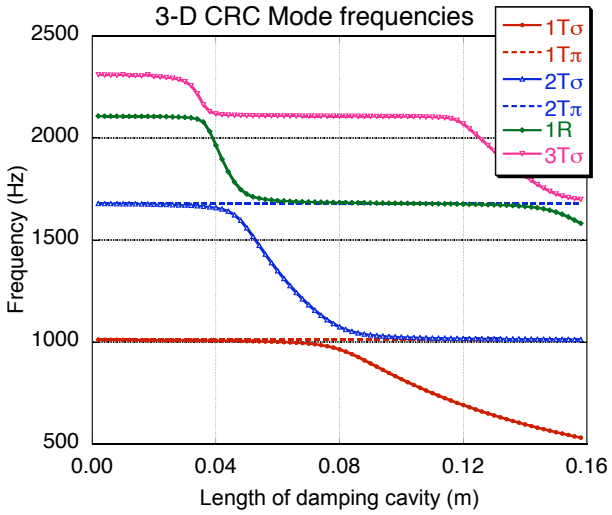

Figure 12: Eigenfrequencies of the first 6 modes of the 3–D CRC as a function of the cavity length

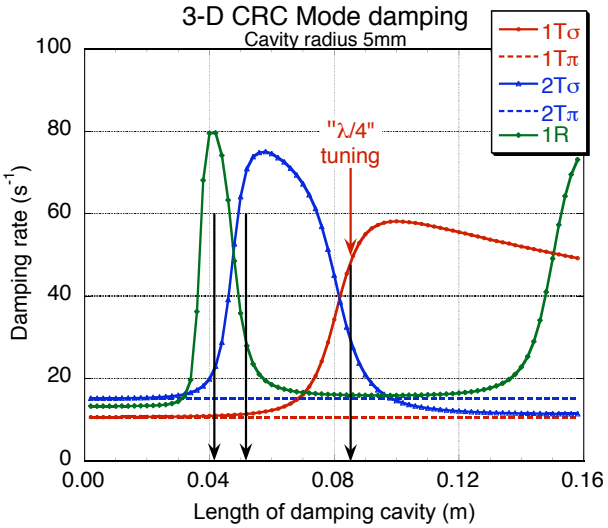

Figure 13: Damping rates of the first 5 modes of the 3–D CRC as a function of the cavity length. All walls are isothermal.

Figure 13 shows the damping rate, σ_p, of the first five modes as a function of the cavity length. Again the behaviour is qualitatively similar to that of the 2–D CRC. The black arrows show the three lengths of the cavities requested for this step. The cavity length $L_R = 41\,\mathrm{mm}$ is well adapted to damp the 1R mode. However it is clear that the cavity lengths $L_R = 51\,\mathrm{mm}$ and $85\,\mathrm{mm}$ are not optimal to damp the $2\mathrm{T}_\sigma$ and $1\mathrm{T}_\sigma$ modes. However, contrary to the 2–D case, there is no single cavity length that provides good damping of both the $2\mathrm{T}_\sigma$ and $1\mathrm{T}_\sigma$ modes. The damping of the $\mathrm{nT}\pi$ modes is insensitive to the length of the damping cavity.

	$L_R = 0\,\text{mm}$		$L_R = 41\,\text{mm}$		$L_R = 51\,\text{mm}$		$L_R = 85\,\text{mm}$		$L_R = 120\,\text{mm}$	
Mode	f Hz	σ_p s^{-1}	f Hz	σ_p s^{-1}	f Hz	σ_p s^{-1}	f Hz	σ_p s^{-1}	f Hz	σ_p s^{-1}
$1T_\sigma$	1009	10.6	1004	11.0	1002	11.3	925	47.8	682	55.5
$1T_\pi$	1009	10.6	1009	10.6	1009	10.6	1009	10.6	1009	10.6
$2T_\sigma$	1675	15.1	1650	21.1	1526	68.0	1042	29.9	1014	12.1
$2T_\pi$	1675	15.1	1675	15.1	1675	15.1	1675	15.1	1675	15.1
1R	2102	13.3	1915	80.3	1711	31.4	1677	16.0	1671	16.4

Table 6: Results for step 4 with cavity lengths = 0 mm, 41 mm, 51 mm, 85 mm, 120 mm and isothermal walls. The eigenfrequencies have been corrected for damping.

The frequencies and damping rates of the first five modes for five selected cavity lengths are given in table 6. In this table the undamped eigenfrequencies of figure 12 have been corrected for damping using the first-order relation $f = f_0 - \sigma_p/(2\pi)$.

7 Discussion

7.1 Are these results reliable?

Yes and No! There is no problem with numerical accuracy: the numerical results agree very closely ($\ll 1‰$) with the analytical solution presented above, when the latter is known (2-D rectangle, 2-D disk, axisymmetric cylinder...). It has been verified that the numerical results are independent of the mesh resolution for the meshes used here. It thus is expected that there is no significant numerical error for the non-trivial geometries

Possible sources of error thus lie in the analytical expressions that have been used to compute the damping rates. The analysis has two components:

- Boundary layer theory
- Eigenmode acoustic analysis

The corresponding analytical expressions are exact, but with a number of restrictions such as:

- No mean flow
- Very small amplitude acoustics
- Small damping rate compared to the frequency

We will first examine the hypotheses and approximations used in the boundary layer theory.

7.2 Approximations and limitations arising from boundary layer theory

1) The boundary layer theory used here supposes that the acoustic pressure and velocity are invariant by translation along the walls. The equivalent approximation is that the acoustic wavelength is very large compared to the boundary layer thickness. This (quasi 1-D) approximation is good for real systems.

2) The boundary layer theory supposes that the acoustic medium is semi-infinite. The equivalent approximation is that the boundary layer thickness negligible compared to all cavity dimensions. This approximation is good for real systems

Other restrictions, not important for test cases here, but which may be important in real systems are:

- Effect of turbulence is neglected. The turbulence level inside damping cavities is low, so this will not be a problem. Elsewhere it is probably not important provided that the Kolmogoroff scale is considerably greater than the acoustic boundary layer thickness.

- Temperature and composition gradients are neglected. The mean-flow boundary layers are much thicker than the acoustic boundary layers, so one should use the gas properties calculated at the wall temperature (supposed known) and not the mean burnt gas properties in the bulk of the chamber.

- The effect of mean flow is neglected. There is no mean flow in damping cavities, so it is not a problem there. However but it will change the calculated contribution of damping by combustion chamber walls.

- The effect of cross flow at cavity exit is neglected. At present I do not know how to estimate eventual errors introduced by this phenomenon.

7.3 Approximations and limitations arising from eigenmode analysis

1) The frequencies given by the Helmholtz solver are (undamped) eigenfrequencies. The real frequencies of damped systems have smaller values. The first order correction for the frequency shift of an acoustic resonator, due to damping, is $f = f_0 - \sigma_p/(2\pi)$, where f_0 is the undamped eigenfrequency. This correction can easily be included. The mode frequencies in tables 2, 3, 4 and 6 have been corrected using this expression.

2) The flowfields are calculated neglecting the flow resistance (due to dissipation) at cavity entrance. The amplitude of the acoustic wave inside the cavity will be over-evaluated when cavity entry resistance is higher than the entry reactance. As a consequence, the damping produced by the cavity walls will also be over-estimated. The expected ratio of over-evaluation is $(R^2 + \chi^2)/\chi^2$ where R and χ are the cavity resistance and reactance. The equivalent cavity entrance resistance can be computed from the dissipation rate and the local acoustic velocity at the cavity entrance [7]. These are known quantities.

3) The Helmholtz equation is exact in the limit of vanishingly small acoustic amplitude. The acoustic flow is then the solution of a potential equation and is thus irrotational. Boundary layer separation and recirculation zones in the acoustic flow are thus totally excluded. For a finite acoustic amplitude, boundary layer separation will occur at sharp edges, such as the exit of a damping cavity. At low to moderate acoustic amplitude, it can be shown that the power is dissipated by recirculation at the cavity exit is negligible in comparison with the dissipation at the chamber walls.

However comparison with numerical simulation shows that boundary layer separation at the cavity exit also modifies the *shape* of the acoustic flow field, and hence the modifies the distribution of velocity and pressure along the walls. Boundary layer separation thus modifies the damping rate by changing the velocity and pressure distribution along the walls. We believe that this phenomenon is responsible for the major part of the difference ($\approx 10\,\%$) between the present results and the CEDRE results of A. Nicole for the geometries of steps 2-4. As a check we have compared our results for step 2 (axisymmetric cavities) when the sharp junction between the two cavities is replaced by a smooth round chamfer. As the radius of the chamfer is increased, the damping rates calculated by the two approaches tend to a common value. When the radius of the chamfer was greater than the diameter of the damping cavity, there was no visible boundary layer separation in the CEDRE simulations (for 10^{-4} relative acoustic amplitude), and the damping rates from the two approaches were in very good agreement.

This unexpected phenomenon is probably the greatest source of error identified so far. The above remarks concerning the comparison between this approach and DNS will also apply to the comparison with experimental measurements on the CRC.

4) In real experiments additional damping may arise from small interstices between modules.

5) In real experiments non-linear damping (acoustic jets) will occur if the acoustic displacement at the cavity exit is of the order, or greater than the cavity radius[14]. This linear limit can also be written $u/\omega > R_{\text{cavity}}$.

Other restrictions, not important for test cases here, but which may be important in real systems are:

- There is no mean flow. It is well-known that resonant frequencies are modified by mean flow in the chamber. Acoustic flow, wall gradients and damping will also be modified It would be possible to account for some Mach effects by solving the aero-acoustic equations instead of the Helmholtz equation. This has not been done yet.
- The analysis has supposed that there is no turbulence and no inhomogeneities. Large scale temperature and density variations can be included in the Helmholtz solver (although it has not been necessary here). However internal damping due to small scale fluctuations cannot be included.
- The effect of an exhaust nozzle was not taken into account. At present it is not possible to model a choked exhaust nozzle. However it is possible to specify an arbitrary wall impedance (if known) in replacement of the nozzle.

8 Conclusions and perspectives

A combination of laminar boundary layer theory and a solver for the Helmholtz equation has been used to provide a simple lightweight method to estimate *linear* damping rate of the test cases proposed in this workshop. The method is applicable to arbitrary complex geometries. The necessary cpu time is of the order of a few seconds for a simple 2-D geometry and of the order of 5 minutes for the 3–D CRC with one damping cavity.

It would not be difficult to apply the method to a combustion chamber equipped with a damping ring of n cavities.

This approach has been validated by DNS for the trivial geometry of a regular cylinder closed at both ends. The approach is strictly laminar, but the thin acoustic boundary layer should remain laminar even for turbulent flows. However the method does not take account effect of boundary layer separation and recirculation on mode shape and velocity distributions. It does not include the contribution of other non-linear phenomena, such as the formation of acoustic jets at high acoustic amplitudes.

The approach can be extended to include space dependant gas properties (temperature, composition). It is also possible to imagine that that this frequency domain approach could be coupled to a time domain code. The frequency domain code could provide damping information to the time domain code (to be modelled by some impedance condition, for example), and the time domain code could provide density and temperature fields for the frequency domain code.

References

[1] D.T. Harrje and F.H. Reardon. Liquid propellant rocket combustion instability. Technical Report SP-194, NASA, Washington, DC, 1972.

[2] V. Yang and A. Anderson. *Liquid rocket engine combustion instability*, volume 169 of *Progress in Astronautics and Aeronautics*. AIAA, Washington DC, 1995.

[3] Uno Ingard and Hartmut Ising. Acoustic nonlinearity of an orifice. *Journal of the Acoustical Society of America*, 42(1):6–17, 1967.

[4] P. K. Tang and W. A. Sirignano. Theory of a generalized helmholtz resonator. *Journal of Sound and Vibration*, 26(2):247–262, 1973.

[5] P. K. Tang, D. T. Harrje, and W. A. Sirignano. Experimental verification of the energy dissipation mechanism in acoustic dampers. *Journal of Sound and Vibration*, 26(2):263–267, 1973.

[6] M.C.A.M. Peters, A. Hirschberg, A.J. Reijnen, and A.P.J. Wijnands. Damping and reflection coefficient measurements for an open pipe at low Mach and low Helmholtz numbers. *Journal of Fluid Mechanics*, 256:499–534, 1993.

[7] Geoffrey Searby, Aurélie Nicole, Mohammed Habiballah, and Emmanuel Laroche. Prediction of the efficiency of acoustic damping cavities. *Journal of Propulsion and Power*, 24(3): 516–523, 2008.

[8] G. G. Stokes. On the communication of vibration from a vibrating body to a surrounding gas. *London, Edinburgh and Dublin Philosophical Magazine and Journal of Science, 4th series*, 36(245):401–421, 1868.

[9] G.K. Batchelor. *An introduction to fluid dynamics*. Cambridge University Press, 1967.

[10] A. K. Nielsen. Acoustic resonators of circular cross-section and with axial symmetry. *Transactions of Danish Academy of Technical Sciences*, 10:9–70, 1949.

[11] H. Tijdeman. On the propagation of sound in cylindrical tubes. *Journal of Sound and Vibration*, 39:1–33, 1975.

[12] Y. Mauriot and A. Nicole. Final report on high frequency combustion instability activities: numerical analysis of chamber acoustics; acoustic cavity investigations; droplet dynamics. Technical Report RT 3/10060 DEFA, ONERA, 2006.

[13] Michael Oschwald, Zoltan Faragó, Geoff Searby, and François Cheuret. Resonance frequencies and damping of a cylindrical combustor acoustically coupled to an absorber. *Journal of Propulsion and Power*, 24(3):524–533, 2008.

[14] I. V. Lebedeva and A. E. Grushin. Amplitude and frequency characteristics of acoustic jets. *Acoustical Physics*, 46(3):359–364, 2003.